Contact-Induced Phase Separation of Alloy Catalyst to Promote Carbon Nanotube Growth

Lu Qiu[1,2] and Feng Ding[1,2,*]

[1]School of Materials Science and Engineering, Ulsan National Institute of Science and Technology, Ulsan 44919, South Korea
[2]Center for Multidimensional Carbon Materials, Institute for Basic Science, Ulsan 44919, South Korea

(Received 5 March 2019; revised manuscript received 7 August 2019; published 18 December 2019)

In this Letter, using density functional theory based molecular dynamics simulations, we report that contact to a carbon nanotube (CNT) induces phase separation in an alloy catalyst, which promotes CNT growth. During growth of a CNT, the growth front tends to preferentially bond to the more active metal atom in the alloy catalyst, thus triggering a phase separation of the alloy catalyst particle. The accumulation of the active metal stabilizes the open end of the CNT, attracts carbon precursors to rapidly diffuse to the growth front, and avoids catalyst poisoning by preventing the encapsulation of the catalyst. This study resolves a long-term mystery surrounding the higher efficiency of alloy catalysts in CNT growth as compared to a pure metal catalyst and thereby paves the way to a more rational catalyst design for controlled CNT growth.

DOI: 10.1103/PhysRevLett.123.256101

Since the seminal observation of Iijima *et al.* in the early 1990s [1,2], despite intense effort from scientists worldwide, a precise structure-controlled growth of carbon nanotubes (CNT) remains elusive. In CNT growth, the catalyst particle serves as a nanoscale template, catalyzes the dissociation of precursors, and controls the diffusion of carbon atoms [3–7]. Thus, it is widely accepted that catalyst design is key to controlling CNT growth.

Experimentally, Fe, Co, Ni [8–9], and other transition metal catalysts [10–16] were used in CNT growth. It has also been observed that, compared to monometallic catalysts, alloy catalysts have significant advantages for CNT growth. In 1997, Fischer and co-workers reported that a mixture of 1 at.% Y and 4.2 at.% Ni resulted in a high yield of single-walled carbon nanotubes (SWNTs) in laser ablation CNT synthesis [17]. Subsequently, by varying the metal composition, various alloy catalysts, such as Fe-Mo, Fe-Ru, Cu-Ni, and Ni-Fe, have been designed to promote CNT growth [18–20]. In addition to high yields, structure-selective synthesis of SWNTs with controlled chirality was also achieved by using alloy catalysts [21–23].

Unlike the case of monometallic catalysts that have been studied using various theoretical methods, including density-functional theory (DFT) [24–28], molecular dynamics (MD) [29–33], or Monte Carlo simulations [34–37], there are no in-depth studies on how an alloy catalyst promotes CNT growth [38]. With the aim of providing a general mechanism to guide alloy catalyst design for CNT growth, we performed systematic DFT-based MD simulations to explore the role of the alloy catalyst in CNT growth. Our results showed that a phase separation occurred in the alloy catalyst, where the more active metal atom tended to concentrate near the CNT-catalyst interface. We also found that this phase separation is critical for highly efficient CNT growth by preventing the closure of the CNT growth front and inhibiting catalyst poisoning.

In our atomic model for DFT-based MD simulations, to reduce computation costs, each metal catalyst, consisting of only 30 atoms, was attached to a short (9,1) tube with a total of 60 C atoms in all simulations. C atoms at the other end of the tube were saturated by hydrogen atoms and fixed during the simulations at 1800 K. All simulations were performed via the Vienna *ab initio* simulation package [39–40] with the projected augmented wave method [41]. To reduce the computational expenses, local density approximation (LDA) was used for the exchange-correlation energy [42], and a relatively small plane-wave cutoff energy of 300 eV and a $1 \times 1 \times 1$ Monkhorst-Pack mesh [43] sampled Brillouin zone were adopted after careful justification of the accuracy (see Supplemental Material [44] Sec. I and Fig. S1).

We first consider a $Au_{15}Ni_{15}$ alloy catalyst particle attached to the open end of a (9,1) SWNT. In the initial configuration [Fig. 1(a)], a random alloy catalyst particle is attached to the rim of the SWNT and both C—Au and C—Ni bonds are formed at the CNT-catalyst interface. During simulation (Supplemental Material [44] Video 1, 1800 K), we clearly see a continuous increase of C—Ni bonds and a concomitant decrease in C—Au bonds [Figs. 1(a)–1(c) and 1(g)], during which the energy of the system continuously decreases [Fig. 1(f)]. The number of C—Ni bonds quickly increases from ∼4 to ∼10 and then rises slowly to ∼12 at 18 ps. Simultaneously, the number of C—Au bonds is progressively reduced and eventually reaches ∼2. The significant increase in C—Ni bonds implies that a preferential grouping of Ni atoms at the CNT-catalyst interface

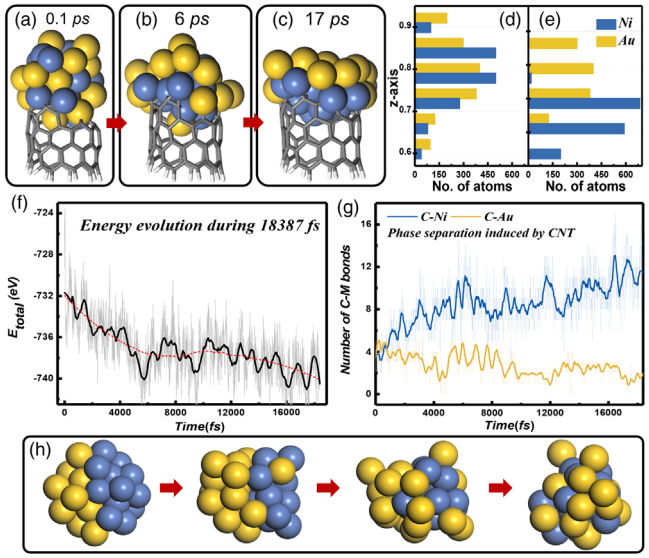

FIG. 1. CNT-induced phase separation during MD simulation of (9,1) tube on $Au_{15}Ni_{15}$ alloy particle at 1800 K. (a) Initial, (b) middle, and (c) final structures of the CNT and alloy particle during MD simulation, where blue and yellow spheres denote Ni and Au metal atoms, and gray and white sticks represent C—C and C—H bonds, respectively. (d) Initial and (e) final metal content distributions along the z direction, where yellow and blue bars represent Au and Ni, respectively. (f) Energy evolution during 18 ps MD simulation. Gray line is the original energy curve, black line is the smoothed line, and the red dashed line highlights the trend of the energy curve. (g) Evolution of the numbers of C—Ni (blue) and C—Au (yellow) bonds during the simulation. (h) Snapshots of the MD simulation of $Au_{15}Ni_{15}$ alloy particle without CNT.

occurs, as clearly depicted in the snapshots of the MD trajectory [Figs. 1(a)–1(c)]. At the end of the MD simulation [Fig. 1(c)], a distinct phase separation of the alloy catalyst particle is seen with Ni atoms forming the bottom part and Au atoms at the top of the catalyst particle, which can be further confirmed by the metal content distributions [Fig. 1(e)]. It is important to note that the tendency in energy change is opposite of the trend in the number of C—Ni bonds, which indicates that a greater number of C—Ni bonds and less C—Au bonds are energetically favored [46–48].

The MD simulation described above clearly demonstrates the phase separation of the alloy catalyst when attached to a growing CNT. To reveal the origin of this phase separation, we consider the evolution of a free-standing alloy catalyst from a phase-separated configuration [Fig. 1(h) and see Supplemental Material [44] Video 4]. During the MD simulation, the two different types of metal atoms gradually mix together [Fig. 1(h)]. The final configuration has more Au atoms on the surface of the particle and more Ni atoms in the central area due to the lower surface energy of Au than that of Ni (see [44] Fig. S2). The energy profile of the trajectory indicates that the formation of the core-shell-like structure is energetically favorable (see [44] Fig. S3). Such a dealloying process must lead to the deactivation of the alloy catalysts since the outer shell of the cluster contains mostly less active metal atoms, which will degrade the catalytic activity of the alloy particle [49–52]. The comparative study shows that phase separation is specific to the alloy catalyst particle attached to the growth front of a CNT; i.e., this phase separation is triggered by the contact between the SWNT and the alloy catalyst and is different from the formation of the core-shell-like structure of the free catalyst particle. This contact-induced phase separation ensures part of the catalyst surface comprises active metal atoms and thus the deactivation of the alloy catalyst for the feedstock decomposition is avoided.

To verify that the contact-induced phase separation is a common phenomenon in CNT growth, we performed MD simulations with four other different types of alloy catalysts ($Au_{10}Ni_{20}$, $Cu_{15}Ni_{15}$, $Cu_{20}Ni_{10}$, and $Fe_{15}Ni_{15}$), among which Cu-Ni [16,53–54] and Fe-Ni [55] are experimentally proven highly efficient alloy catalysts for CNT growth. Detailed analyses of the MD simulations are presented in the Supplemental Material [44] (Figs. S4–S9, Videos 2, 3, 5, and 6), from which the contact-induced phase separation is clearly seen in all alloy catalysts. So, we conclude that the accumulation of active metal atoms at the CNT-catalyst interface is a common phenomenon in alloy particle catalyzed CNT growth.

It is worth noting that an alloy catalyst that contains one metal that can easily form a high stable carbide phase cannot be considered as a simple bimetal alloy as discussed above. Such as in the CoMoCat CNT growth, the active Mo atoms will first form a carbide phase and release Co particles as an active catalyst for CNT growth [21]. In such a process, the strong binding between CNT and Mo atoms is greatly reduced after the formation of the Mo carbide phase, and therefore, the active and less active metal phase in the alloy is inversed (see [44] Sec. VIII and Fig. S10).

Next, we investigated whether such a phase separation is also found in large alloy particles, for which sizes could be as high as 10 nm in real CNT growth experiments. DFT-based MD simulations of such a large system ($\sim 10^5$ atoms) is not realistic, [29,34,37] and therefore, we focused only on a small part of the tube-catalyst interface. As shown in Fig. 2(a), a small part of the CNT-catalyst interface is modeled by an attached graphene sheet (with armchair edge) that is perpendicular to a flat Au-Ni alloy slab surface. From Figs. 2(b)–2(e), we see that there is no Ni atom directly attached to the edge of graphene in the initial configuration, but during the simulation, the number of Ni atoms around the graphene edge increases continuously. After ~15 ps MD simulation (see Supplemental Material [44] Video 7), the aggregation of Ni atoms at the interface is clearly seen [Figs. 2(e) and 2(g)]. Further simulations with

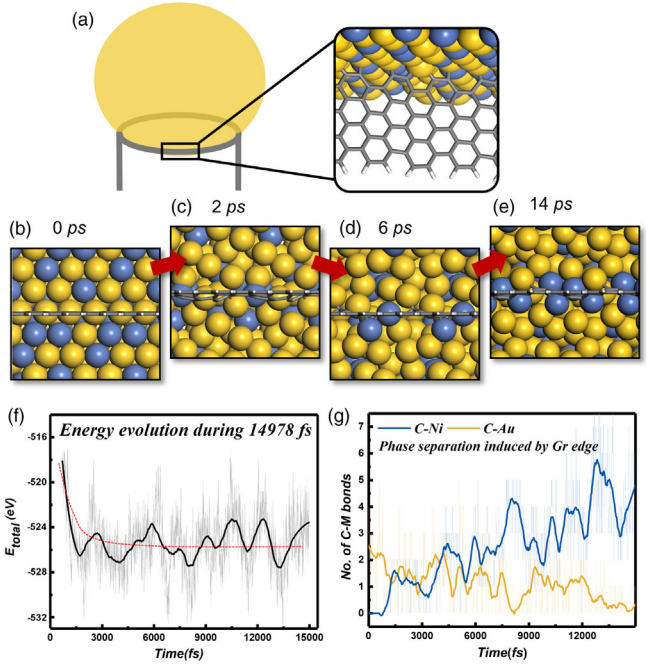

FIG. 2. Phase separation in a large system. (a) Schematic diagram illustrating that, in a large system, at the interface between alloy particle and CNT, the model could be viewed as a graphene edge perpendicularly attached to the flat alloy surface. Blue and yellow spheres are Ni and Au atoms, while gray and white sticks are C—C and C—H bonds. (b)–(e) Snapshots (top views) during 15 ps MD simulation. (f) Energy evolution during the MD simulation, where gray line is the original energy curve, black line is the smoothed curve, and red line shows the trend in energy change. (g) Evolution of the numbers of C—Ni (blue) and C—Au (yellow) bonds during the simulation.

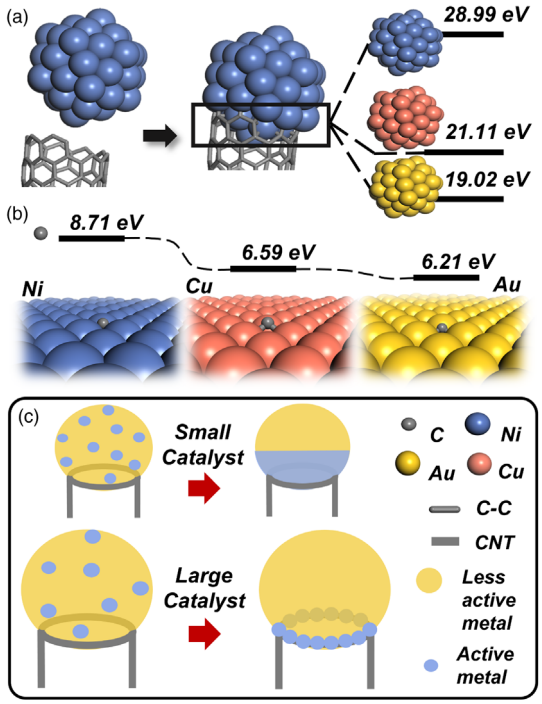

FIG. 3. Illustration showing the underlying mechanism of the contact-induced phase separation of an alloy catalyst. (a) Binding energies of Ni_{55}, Cu_{55}, and Au_{55} catalysts to a (9,1) CNT. (b) Binding energies between C atom and Ni(111), Cu(111), Au(111) surfaces. (c) Schematic diagram showing the phase separation in both small (diameter ≈1 nm) and large (diameter >2 nm) catalysts.

a graphene zigzag edge attached to Au-Ni and Cu-Ni alloy catalyst surfaces (see Supplemental Material [44] Fig. S11 and Videos 8 and 9) exhibit the same tendency, where Ni atoms preferentially aggregate in the vicinity of the graphene-catalyst interface.

The above simulations unequivocally show that the CNT-catalyst contact induces a phase separation of the alloy and that the active catalyst atom tends to aggregate near the CNT-catalyst interface during the alloy-catalyzed CNT growth [56]. For small catalysts [Fig. 3(c), top], the active metals will segregate to the bottom of the particle to interact with the growing CNT; for large catalyst particles [Fig. 3(c), bottom], the phase separation can be realized through the accumulation of the active metal at the tube-catalyst interface, forming a circular ring of active metal atoms attached to the open end of the CNT (Fig. 2 and see Supplemental Material [44] Fig. S11).

To obtain a deeper understanding of the phase separation of the alloy catalyst, we have analyzed the interaction between a CNT and different transition metals. DFT calculations show that a (9,1) CNT adheres to Ni_{55}, Cu_{55}, and Au_{55} particles with binding energies of 29, 21, and 19 eV, respectively [Fig. 3(a)], indicating that Ni is the most active and Au is the least active in its interaction with a CNT. Hence, it is not surprising that the aggregation of the more active metal atoms at the CNT-catalyst interface to form strong C-metal bonds will reduce the total energy of the system. One consequence of this effect is that the formation of strong C-metal bonds at the CNT-catalyst interface would further stabilize the open end of the CNT, which is essential for the continuous growth of CNTs [46–48]. Considering a relatively large alloy catalyst particle of ∼5 nm, with ∼10 000 atoms, a few percent of active metal atoms (e.g., ∼200) is sufficient to terminate the open end of a 2–3 nm diameter CNT. Thus, using an alloy catalyst with a large number of less active metal atoms and a small amount of more active metal atoms for CNT growth is feasible [15–16].

In addition to effectively terminating the growing CNT, we have also investigated how the phase separation affects CNT growth by carrying out further MD simulations while adding C atoms to the phase-separated catalyst particle. As shown in Fig. 4(c), 15 C atoms are randomly added onto the surface of a $Au_{15}Ni_{15}$ alloy catalyst particle. A few pico-seconds later, most of the C atoms added to the Au part diffuse to the Ni part, which is closer to the CNT-catalyst interface because of the stronger C—Ni bonding than the C—Au bonding [Figs. 3(a) and 3(b)]. As a consequence of

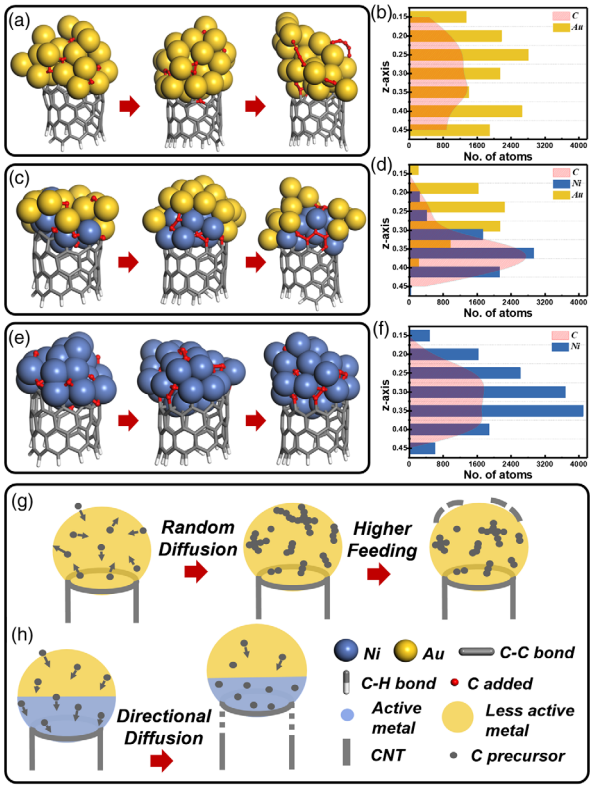

FIG. 4. CNT growth on a phase-separated alloy catalyst and on normal monometallic catalysts. Snapshots taken at initial, middle, and final stages of the MD simulations of (9,1) CNT on (a) Au, (c) $Au_{15}Ni_{15}$ alloy, and (e) Ni particles. Atom distributions along the z direction at the end of the simulations (last 5 ps) for (b) Au, (d) $Au_{15}Ni_{15}$ alloy, and (f) Ni particles. Red shaded area denotes the distribution of C atoms; yellow and blue bars are for Au and Ni atoms, respectively. Schematic diagrams showing CNT growth with (h) alloy and (g) monometallic catalysts.

the directional C diffusion on the catalyst surface, the precursor concentration at the CNT-catalyst interface becomes very high [Fig. 4(d)] and must lead to the fast growth of the CNT. As evident in our MD simulation, a new hexagon is formed at the open end of the CNT. It is important to note that the catalyst remains phase separated even with the further addition of C atoms, as shown in the atom distribution profile [Fig. 4(d)].

To make a comparison, similar MD simulations were carried out to explore the tube growth with two pure metal particles, Au_{30} and Ni_{30}. It can be clearly seen that the distributions of the C atoms on the homogeneous metal catalyst surfaces show no change [Figs. 4(a), 4(b), 4(e), and 4(f)]. During the simulations, we observe that a few C atoms get attached to the rim, but no complete polygonal ring is formed. In addition to the slow addition of C atoms to the SWNT, carbon chains of different lengths are observed on the catalyst surface [31–33], which is in sharp contrast to the clean top surface of the Au-Ni alloy particle.

Our results thus show conclusively that there are two advantages of using alloy catalysts in CNT growth as compared to pure catalysts. First, the strong binding between the active metal and the carbon precursor [Fig. 3(b)] will lead to a directional diffusion of the C precursor to the part of the catalyst with the more active metal very close to the growth front of the CNT [Fig. 4(h)], which leads to a higher precursor concentration at the CNT-catalyst interface [Fig. 4(d)]. Thus, a fast CNT growth is achieved [Fig. 4(h)]. In contrast, on a pure metal particle surface, there is an even distribution of the precursors on the whole surface, which should result in a relatively slow growth rate [Fig. 4(g)]. If the C feeding rate is further increased, the high concentration of C atoms at the top of the catalyst may initiate the nucleation of a large carbon cluster, just like the carbon chains observed in the simulations [Fig. 4(a)], and even new sp^2 networks, which are well known to poison the catalyst by forming a graphitic layer encapsulating the particle [30,47,57–58]. In contrast, as compared to a pure metal catalyst, the top side of the alloy catalyst is less active and the concentration of carbon precursors is much lower, which prevents catalyst encapsulation and thus prolongs SWNT growth. With a faster growth rate and longer growth time, it is certain that the yield of CNTs will be greatly increased.

In summary, using DFT-based MD simulations of CNT growth, we observed CNT-induced phase separation of the alloy catalysts. The active metal atom tends to move toward the open end of the CNT, and this induces a phase separation of the alloy particle into an active part and a less active part, which prevents the deactivation of the alloy catalysts. The accumulated active metal atoms at the tube-catalyst interface attracts C precursors to diffuse quickly toward the growth front of the CNT, resulting in faster CNT growth. Additionally, the gathering of the less active metal atoms on the top side of the catalyst prevents the termination of the CNT growth by avoiding graphitic encapsulation of the catalyst. It should be noted that the activity of a metal depends on the reaction environment of CNT growth, where some metals may easily form carbide phases [21,59] and the weak binding between CNTs and the metal carbide may greatly reduce the activity of the corresponding metal. For example, Mo atoms are more active than Co atoms in a Co-Mo alloy catalyst. While, during CNT growth, Co becomes more active for CNT growth after Mo atoms form a stable Mo carbide phase. So, the CNT will be terminated by the Co and the Mo carbide will be at the other side of the catalyst particle [60–61]. This study clearly reveals an advantage of using alloy catalysts for CNT growth, and the contact-induced phase separation of the alloy catalysts can be considered as a general rule to guide catalyst design for controllable CNT growth. Here we would like to note that the contact-induced phase separation in an alloy catalyst might be not the only advantage for CNT growth. As demonstrated before, alloy catalysts may have several other advantages for the CNT growth, such as the reduced melting point of the catalyst particle [62], reduced eutectic

point with tunable carbon solubility of the carbon-alloy system [63], and the formation of metal carbide as a part of the catalyst particle demonstrated in the W-Co alloy recently [59].

The authors acknowledge support from the Institute for Basic Science (IBS-R019-D1) of South Korea and the Outstanding Research Fund (1.170072.01) of Ulsan National Institute of Science and Technology.

*f.ding@unist.ac.kr

[1] S. Iijima, Nature (London) **354**, 56 (1991).
[2] S. Iijima, and T. Ichihashi, Nature (London) **363**, 603 (1993).
[3] A. Moisala, A. G Nasibulin, and E. I. Kauppinen, J. Phys. Condens. Matter **15**, S3011 (2003).
[4] A. C. Dupuis, Prog. Mater. Sci. **50**, 929 (2005).
[5] S. Irle, Y. Ohta, Y. Okamoto, A. J. Page, Y. Wang, and K. Morokuma, Nano Res. **2**, 755 (2009).
[6] A. R. Harutyunyan, J. Nanosci. Nanotechnol. **9**, 2480 (2009).
[7] O. V. Yazyev and A. Pasquarello, Phys. Rev. Lett. **100**, 156102 (2008).
[8] D. S. Bethune, C. H. Kiang, M. S. de Vries, G. Gorman, R. Savoy, J. Vazquez, and R. Beyers, Nature (London) **363**, 605 (1993).
[9] W. Z. Li, S. S. Xie, L. X. Qian, B. H. Chang, B. S. Zou, W. Y. Zhou, R. A. Zhao, and G. Wang, Science **274**, 1701 (1996).
[10] D. Takagi, Y. Homma, H. Hibino, S. Suzuki, and Y. Kobayashi, Nano Lett. **6**, 2642 (2006).
[11] Y. Qian, C. Wang, G. Ren, and B. Huang, Appl. Surf. Sci. **256**, 4038 (2010).
[12] B. Liu, W. Ren, L. Gao, S. Li, Q. Liu, C. Jiang, and H.-M. Cheng, J. Phys. Chem. C **112**, 19231 (2008).
[13] Y. Li, R. Cui, L. Ding, Y. Liu, W. Zhou, Y. Zhang, Z. Jin, F. Peng, and J. Liu, Adv. Mater. **22**, 1508 (2010).
[14] D. Yuan, L. Ding, H. Chu, Y. Feng, T. P. McNicholas, and J. Liu, Nano Lett. **8**, 2576 (2008).
[15] W. Zhou, Z. Han, J. Wang, Y. Zhang, Z. Jin, X. Sun, Y. Zhang, C. Yan, and Y. Li, Nano Lett. **6**, 2987 (2006).
[16] S. Bhaviripudi, E. Mile, S. A. Steiner, A. T. Zare, M. S. Dresselhaus, A. M. Belcher, and J. Kong, J. Am. Chem. Soc. **129**, 1516 (2007).
[17] C. Journet, W. K. Maser, P. Bernier, A. Loiseau, M. Lamy de la Chapelle, S. Lefrant, P. Deniard, R. Lee, and J. E. Fischer, Nature (London) **388**, 756 (1997).
[18] A. M. Cassell, J. A. Raymakers, J. Kong, and H. Dai, J. Phys. Chem. B **103**, 6484 (1999).
[19] N. K. Memon, B. H. Kear, and S. D. Tse, Chem. Phys. Lett. **570**, 90 (2013).
[20] M. Yudasaka, Y. Kasuya, F. Kokai, K. Takahashi, M. Takizawa, S. Bandow, and S. Iijima, Appl. Phys. A **74**, 377 (2002).
[21] S. M. Bachilo, L. Balzano, J. E. Herrera, F. Pompeo, D. E. Resasco, and R. B. Weisman, J. Am. Chem. Soc. **125**, 11186 (2003).
[22] X. Li, X. Tu, S. Zaric, K. Welsher, W. S. Seo, W. Zhao, and H. Dai, J. Am. Chem. Soc. **129**, 15770 (2007).
[23] F. Yang, X. Wang *et al.*, Nature (London) **510**, 522 (2014).
[24] Q. Yuan, H. Hu, and F. Ding, Phys. Rev. Lett. **107**, 156101 (2011).
[25] Y. H. Lee, S. G. Kim, and D. Tomanek, Phys. Rev. Lett. **78**, 2393 (1997).
[26] F. Ding, A. R. Harutyunyan, and B. I. Yakobson, Proc. Natl. Acad. Sci. U.S.A. **106**, 2506 (2009).
[27] V. I. Artyukhov, E. S. Penev, and B. I. Yakbson, Nat. Commun. **5**, 4892 (2014).
[28] Z. Xu, L. Qiu, and F. Ding, Chem. Sci. **9**, 3056 (2018).
[29] Z. Xu, T. Yan, and F. Ding, Chem. Sci. **6**, 4704 (2015).
[30] F. Ding, K. Bolton, and A. Rosen, J. Phys. Chem. B **108**, 17369 (2004).
[31] Y. Ohta, Y. Okamoto, S. Irle, and K. Morokuma, ACS Nano **2**, 1437 (2008).
[32] Y. Ohta, Y. Okamoto, S. Irle, and K. Morokuma, J. Phys. Chem. C **113**, 159 (2009).
[33] Y. Ohta, Y. Okamoto, S. Irle, and K. Morokuma, Carbon **47**, 1270 (2009).
[34] M. Diarra, A. Zappelli, H. Amara, F. Ducastelle, and C. Bichara, Phys. Rev. Lett. **109**, 185501 (2012).
[35] M. He *et al.*, Nanoscale **10**, 6744 (2018).
[36] M. He, Y. Magnin, H. Amara, H. Jiang, H. Cui, F. Fossard, A. Castan, E. Kauppinen, A. Loiseau, and C. Bichara, Carbon **113**, 231 (2017).
[37] U. Khalilov, A. Bogaerts, and E. C. Neyts, Nat. Commun. **6**, 10306 (2015).
[38] E. S. Penev, K. V. Bets, N. Gupta, and B. I. Yakobson, Nano Lett. **18**, 5288 (2018).
[39] G. Kresse and J. Hafner, Phys. Rev. B **48**, 13115 (1993).
[40] G. Kresse and J. Furthmüller, Comput. Mater. Sci. **6**, 15 (1996).
[41] G. Kresse and D. Joubert, Phys. Rev. B **59**, 1758 (1999).
[42] J. P. Perdew and A. Zunger, Phys. Rev. B **23**, 5048 (1981).
[43] H. Monkhorst and J. Pack, Phys. Rev. B **13**, 5188 (1976).
[44] See Supplemental Material at http://link.aps.org/supplemental/10.1103/PhysRevLett.123.256101 for the validation of the accuracy of using the LDA method, the estimated surface energy of Au, Cu, Ni, and Fe, the simulation of the $Au_{20}Ni_{10}$ alloy catalyst without CNT, the phase separation of $Au_{10}Ni_{20}$, $Cu_{15}Ni_{15}$, $Cu_{20}Ni_{10}$, and $Fe_{15}Ni_{15}$ alloy catalyst during CNT growth, binding energies between CNT and Co_{55}, Mo_{55}, and $Mo_{55}C_{18}$ particles, the phase separation of large alloy systems, and the caption for videos of the MD simulations, which includes Ref. [45].
[45] A. K. Kumikhov and K. B. Khkhonov, J. Appl. Phys. **54**, 1346 (1983).
[46] F. Ding, P. Larsson, J. A. Larsson, R. Ahuja, H. Duan, A. Rosén, and K. Bolton, Nano Lett. **8**, 463 (2008).
[47] M. A. Ribas, F. Ding, P. B. Balbuena, and B. I. Yakobson, J. Chem. Phys. **131**, 224501 (2009).
[48] J. Robertson, J. Mater. Chem. **22**, 19858 (2012).
[49] T. S. Cale and J. T. Richardson, J. Catal. **79**, 378 (1983).
[50] N. M. Rodriguez, M. S. Kim, and R. T. K. Baker, J. Catal. **140**, 16 (1993).
[51] P. Strasser and S. Kuhl, Nano Energy **29**, 166 (2016).

[52] Y. Shen *et al.*, Catal. Sci. Technol. **8**, 3853 (2018).
[53] H. Y. Miao, J. T. Lue, S. Y. Chen, S. K. Chen, and M. S. Ouyang, Thin Solid Films **484**, 58 (2005).
[54] W. J. Jong, S. H. Lai, K. H. Hong, H. N. Lin, and H. C. Shih, Diam. Relat. Mater. **11**, 1019 (2002).
[55] W.-H. Chiang and R. M. Sankaran, Nat. Mater. **8**, 882 (2009).
[56] M. He, H. Jin *et al.*, Carbon **110**, 243 (2016).
[57] J. Zhao, A. Martinez-Limia, and P. B. Balbuena, Nanotechnology **16**, S575 (2005).
[58] Y. Shibuta and S. Maruyama, Chem. Phys. Lett. **382**, 381 (2003).
[59] H. An *et al.*, Sci. Adv. **5**, eaat9459 (2019).
[60] J. E. Herrera, L. Balzano, A. Borgna, W. E Alvarez, and D. E Resasco, J. Catal. **204**, 129 (2001).
[61] A. Monzon, G. Lolli, S. Cosma, S. B. Mohamed, and D. E. Resasco, J. Nanosci. Nanotechnol. **8**, 6141 (2008).
[62] Y. Nakayama, L. Pan, and G. Takeda, Jpn. J. Appl. Phys. **45**, 369 (2006).
[63] T. Wu *et al.*, Nat. Mater. **15**, 43 (2016).